DISCRETE ELEMENT ANALYSIS ON THE INFLUENCE OF DRILLING FLUID PRESSURE ON CORE DISCING IN PRESSURE-PRESERVED CORING

by

Ding-Ming WANG[a], Ling CHEN[b*], Da GUO[b], Zhi-Qiang LIU[c], Ju LI[b], Xun YANG[b], and Yi-Wei ZHANG[a]

[a]College of Water Resource and Hydropower, Sichuan University, Chengdu, China
[b]School of Mechanical Engineering, Sichuan University, Chengdu, China
[c]JinshiDrilltech Co. Ltd., Tangshan, China

Original scientific paper
https://doi.org/10.2298/TSCI2301655W

In the process of coring in a high in-situ stress environment, the rock core is damaged due to stress release, and core discing is a prominent manifestation of this damage. Pressure-preserved coring has no direct effect on in-situ stress, and its influence on stress release is related to drilling fluid pressure. Yet fluid pressure in the coring process was not considered in most former numerical simulation studies on core discing. In this paper, the discrete element method software PFC3D is used to conduct a numerical simulation of the coring process. According to the two conditions without drilling fluid pressure and with it, and different horizontal in-situ stresses of 5-160 MPa, fracture and discing of the core with drilling are observed. In addition, the law of fracture and discing in the process of coring was studied, and the function of pressure-preserved coring to prevent fracture and discing is explored. Simulation results show nonlinear trends in distribution of discs both in time and in space.

Key words*: pressure-preserved coring, core discing, discrete element, drilling fluid pressure*

Introduction

In-situ pressure-preserved coring is an effective method used in many deep mining situations [1, 2], and was helpful in many field tests [3-6], including the influence on core discing. Core discing is a very obvious and intuitive phenomenon that may occur in the process of coring under high stress environment. In the early stage, Jaeger and Cook studied discing the phenomenon in 1963 [7], believing that core discing is caused by tensile failure. Matsuki *et al.* [8] also proposed a linear formula with tensile strength. Since researchers have been trying to find its relationship with in-situ stress, a kind of *physiognomy* with core discing as an object was put forward [9]. Discs have several types but are often saddle-shaped, Matsuki *et al.* [8] found the relationship between the axis of the saddle and the maximum horizontal principal stress. On the other hand, Obert [10] initially suggested that the higher

[*]Corresponding author, e-mail: chenlingscu@scu.edu.cn

stress, the thinner the core disc. Haimson [11] confirmed the relationship between the length of discs and the magnitude of stress through experiments.

In addition to some field and laboratory studies [12], most researchers used numerical simulation methods. Li Y *et al.* [13] explored stress concentration and crack development in the process of coring by using FEM. Hakala [14] and Yameogo *et al.* [15] also used 3-D FEM to study the relationship between core damage and in-situ stress. In terms of DEM [16], Bahrani *et al.* [17] used PFC2D to explore the stress variation in the process of coring. Since a large number of FEM models have been tried for core discing and in-situ stress, the DEM may provide a new way.

In this paper, a software PFC3D has been used to build a model, which reflected the coring process and collected information related to core discing. The specific coring process and drilling environment were not considered in most of former numerical simulation studies on core discing, especially the drilling fluid pressure, which has a marked influence on core failure [18]. The coring process with one of two conditions, with drilling fluid pressure or without it, was simulated on this paper's model.

The PFC model establishment

Considering insufficient compression to tensile stress, σ_c/σ_t, in most PFC models, the flat-joint model which has a σ_c/σ_t of 8-9 is adopted in this paper. The parameters of PFC model only reflect the properties of individual particles and contacts, of which the change with the macroscopic parameters of rock is non-linear and non-orthogonal. Parameter calibration has been only conducted by manual adjustment. Therefore, the calibration code is optimized to repeat the cycle to simulate the test and modify the input parameters according to the comparison of the result with macroscopic parameters, until the maximum deviation is satisfied.

Table 1 shows the target value and deviation of macroscopic parameters, and the value of the final calibrated mesoscopic parameters. The target values of macroscopic parameters are taken from the general rock mechanical parameters of granite. From the results, the macro parameters obtained by simulation are very close to the target value, and the maximum deviation is less than 0.0085.

Table 1. Parameters of rock and mesoscopic parameters in PFC

				Parameters in PFC		
Parameter	Symbol	Value	Deviation	Parameter	Symbol	Value
Elastic modulus	E	26 GPa	–0.0064	Effective modulus	E'	24.7 GPa
Poisson's ratio	μ	0.22	–0.0032	Stiffness ratio	κ	3.5166
Tensile strength	σ_t	9 MPa	0.0081	Tensile strength	σ_c'	13.2 MPa
Cohesion	c	14.3 MPa	–0.0085	Cohesion	c'	36.5 MPa
Friction angle	ϕ	54°	–0.0077	Friction angle	ϕ'	52.916°
Compressive strength	σ_{ucs}	80 MPa	–	Friction coefficient	μ'	0.5

The DEM simulation model is shown in fig. 1. The rock body is a 100 × 100 × 330 mm cube. To ensure efficiency, the minimum particle radius is set as 1.3 mm, and the maximum radius is 1.66 times of the minimum radius. Radial and axial confining pressures are first applied to the model to make it in an in-situ stress environment. After stabilization, a new circular boundary with a diameter of 65 mm was demarcated in the center of the top boundary before coring, and the confining pressure applied on this boundary was adjusted to 0, as shown in fig. 2.

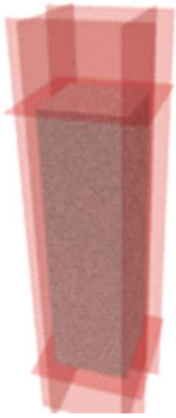

Figure 1. The PFC rock model and boundary conditions

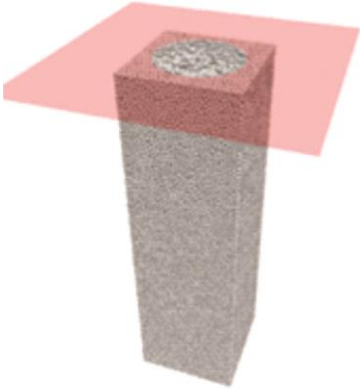

Figure 2. Making a borehole on the top of the model

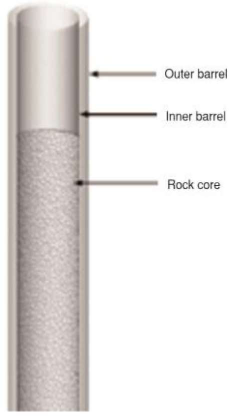

Figure 3. Construction of coring tool

In the most of former studies of core discing simulation using discrete elements, particles outside the core boundary were directly deleted to result in stress release. In this paper, a coring tool is designed to simulate the real coring process as much as possible, as shown in fig. 3. The coring tool is composed of two cylinders. The diameter of the outer cylinder is 65 mm and that of the inner cylinder is 50 mm. In coring process, when the rock core enters the inner cylinder, and the axial and radial pressure applied to the core can be controlled to simulate the effect of drilling fluid.

Although the entity of the coring tool is constructed in this paper, it is also simplified to ensure calculation efficiency. For example, particles the of rock model would not be destroyed because of rotating cutting of the bit, but would be removed when the axial contact force between the particle and the bit part reaches a certain value during drilling. The drilling speed is determined by the maximum contact force between a single particle and the bit. This implies that:

$$v_{\text{drill}} = \frac{1-k_F}{\mathrm{e}^{k_F}}(v_{d,\max} - v_{d,\min}) + v_{d,\min}$$
$$k_F = \frac{F_b}{F_c} \tag{1}$$

where v_{drill} is the drilling speed, F_c – the axial contact force threshold of deleting the particle, F_b – the maximum axial contact force of all particles in contact with the drill, $v_{d,\min}$ and $v_{d,\max}$ are the minimum and maximum value of the drilling speed, $v_{d,\min}$ is close to the drilling speed of normal coring. When the bit is not in full contact with particles, or the contact force, F_b is very small, the drilling speed, and v_{drill} would exceed the normal coring speed, in order to reduce meaningless calculation.

Since the ratio between horizontal and vertical in-situ stress has an influence on core discing, and the ratio of horizontal and vertical stresses σ_H/σ_v varies greatly in different geologic environments. For comparison purposes, σ_H/σ_v is set to 2. The pressure of drilling fluid σ_L is given:

$$\sigma_L = 0.5\frac{\rho_L}{\rho_R}\sigma_v \tag{2}$$

where ρ_L and ρ_R are the drilling fluid density and the average density of the overlying rock mass. In this paper, we set ρ_L = 1000 kg/m^3 and ρ_R = 2650 kg/m^3.

In this model, the core length is planned to be 300 mm. After the coring tool reaches this depth, in order to make the core completely enter the inner cylinder, the coring tool would advance at the original speed for a certain time, and the specific depth depends on the drilling speed at this time. In the simulation conducted in this paper, the excess depth is about 10 ±1 mm.

At the end of drilling, each individual fragment separated from the other is recorded according to the position and connection of each particle in the core. Moreover, different particle number thresholds were set to count the fragments whose particle number was greater than the threshold, and the obtained value $N_f^{[i]}$ could judge the extent of core discing. In the cores obtained in this paper, the N_f recorded in each simulation is set as $N_f^{[1]}$, $N_f^{[20]}$ (1/5 of the number of particles in one layer) and $N_f^{[64]}$ (2/3 of the number of particles in one layer).

In the simulation with or without drilling fluid pressure, in order to increase the sampling points in the pressure range where the extent of discing changes greatly, the bisection value of 5 MPa ≤ σ_H ≤ 140 MPa is conducted with $N_f^{[20]}$ as the judgment benchmark, and the increasing uniform value of 10 MPa is supplemented.

Simulation results with drilling fluid pressure

As aforementioned, in the simulation with drilling fluid pressure, pressure is applied to the core using the inner cylinder of the coring tool, which is linearly related to the vertical in-situ stress σ_v and the horizontal in-situ stress σ_H.

Figure 4(a) shows the variation of fracture number with drilling depth under different σ_H. Under various in-situ stress conditions, the number of fractures increases linearly, which is the same as the case without drilling fluid pressure. As shown in the figure, the number of fractures also decreases at low stress. When it is above 20 MPa, fractures increase with the increase of in-situ stress. Figure 4(b) shows the number of fractures with different σ_H after drilling. Within the sampling range, there are two zones where the difference in the number of fractures between the two conditions is most significant: one is the valley near 20 MPa, and the other one is the sampling point with the greatest in-situ stress. On the other hand, in the middle of two curves, fractures in these two cases are almost equal, and even the number of fractures with fluid pressure exceeds that without drilling fluid pressure.

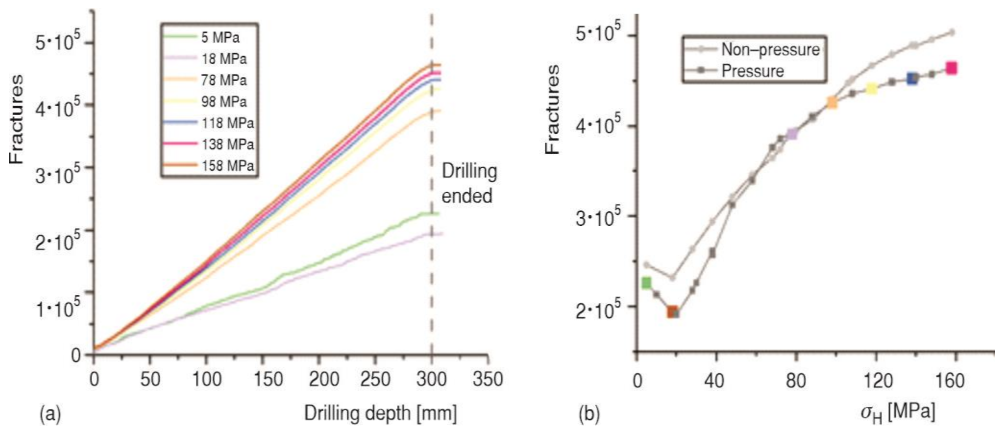

Figure 4. Number of fractures in drilling process and fractures when drilling ended; (a) drilling process with drilling fluid pressure and (b) drilling ended

As in the previous section, three kinds of fragment quantity are also obtained in simulations with drilling fluid pressure. Figure 5 reflects the model and the curves of the number of fragments at the end of drilling under the two conditions when the horizontal in-situ stress is 68 MPa. When σ_H reaches 68 MPa, the number of fractures is lower without fluid pressure, which is also intuitively reflected in fig. 5(b). However, the following chart shows slightly different contents. For, $N_f^{[i]}$ fragments without drilling fluid pressure are 754 higher than that with fluid pressure. For, $N_f^{[64]}$ the final results in the two cases are approximately equal. The $N_f^{[20]}$ with drilling fluid pressure is twice than that without fluid pressure.

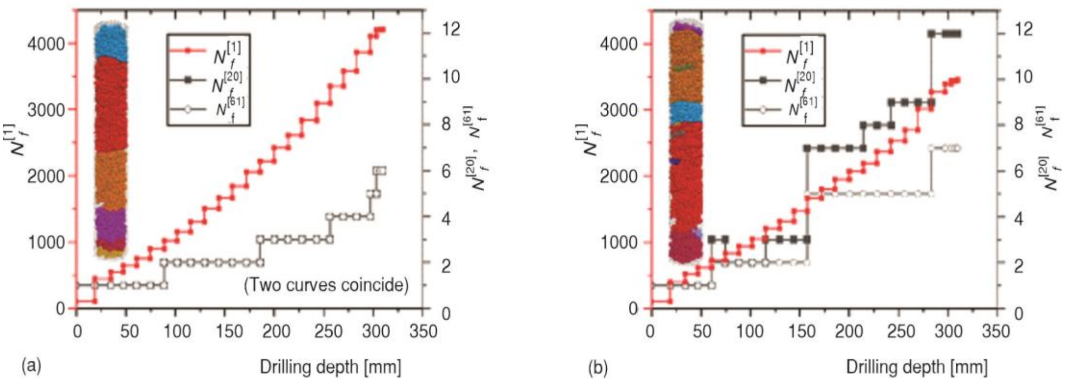

Figure 5. Model and fragment number with the absence and the presence of drilling fluid pressure; (a) σ_H = 68 MPa, σ_L = 0 MPa and (b) σ_H = 68 MPa, σ_L = 6.42 MPa

Discussions

Description of core discing during drilling

The aforementioned drilling depth, is a time-dependent quantity that indicates the depth of the bottom of the coring tool in drilling process. It differs from the core depth, *i.e.*, the axial position of the core at the end of drilling. These two quantities can be used to analyze the height of changes occurring in the core relative to the bit position. For example, Figure 6(a) shows two fracture number curves without drilling fluid under σ_H = 98 MPa. In most cases, fractures of drilling depth were slightly greater than fractures of core depth, indicating that some fractures had occurred below the coring tool during drilling. The difference of fractures with drilling depth to that with core depth is shown in Figure 6(b), which rises at the beginning, then gradually decreases to about 8000, and then drops sharply. The descent begins at a depth of approximately 280 mm, indicating that most of the fracture below the coring tool occurs within 20 mm. At a depth of 300 mm, the difference is less than 0 near the depth of 300 mm, about -1000, and gradually reaches 0 after 300 mm. This indicates that a fraction of fractures occurred after drilling, however, this fraction is very small compared to the total amount of fractures. In other words, in the absence of drilling fluid pressure, most fractures occur while drilling.

On the other hand, fragment quantities with drilling depth reflects the extent of core discing at a certain point in the drilling process. Figure 7 shows the corresponding relationship between the core model without drilling fluid pressure when σ_H reaches 98 MPa and $N_f^{[20]}$ of that. As can be seen from the figure, the variation of $N_f^{[20]}$ at lower drilling depths is consistent with the fragmentation of the core model, that is, several large fragments in the upper part of the core are generated immediately during drilling. At the end of the curve, the rise after 300 mm indicates that some new fragments are generated after the core enters the core barrel, but most of them are concentrated near the bottom of the core.

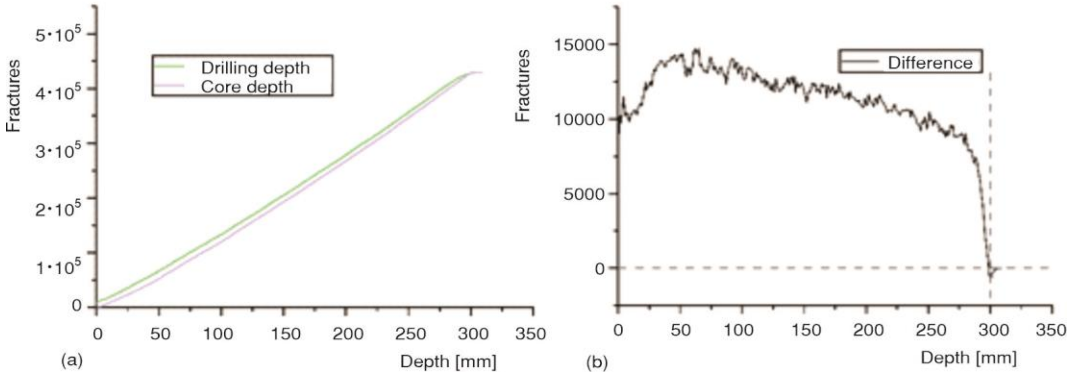

Figure 6. Fractures and difference with drilling depth and core depth, of which horizontal in-situ stress equals 98 MPa; (a) fractures with drilling depth and core depth and (b) difference of fractures with drilling depth to that with core depth

Influence of drilling fluid pressure on core discing

In simulations presented in this paper, the relationship between drilling fluid pressure and in-situ stress is set to be linear, but according to the results shown in fig. 4(b), the effect of drilling fluid pressure on core fractures is non-linear. If with the same number of fractures, the horizontal in-situ stress with fluid pressure is σ_H, while that without fluid pressure is σ_H' Then $\sigma_H - \sigma_H'$ represents the ability of drilling fluid pressure to suppress core fracture caused by in-situ stress, of which the curve and σ_L is shown in fig. 8. It can be seen that, the difference decreases first and then rises, and the part less than 0 indicates that the fluid pressure has a negative effect. Only when the horizontal ground stress is greater than 100 MPa, the difference begins to rise close to a linear trend.

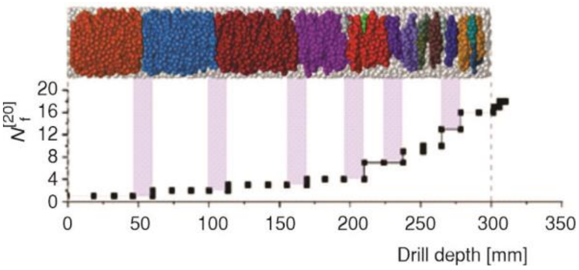

Figure 7. Comparison of the model and fragment quantity without drilling fluid pressure, of which horizontal in-situ stress equals 98 MPa

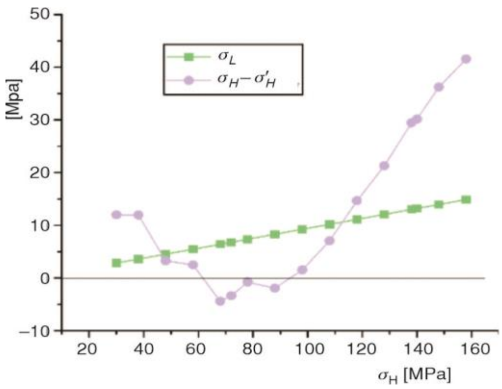

Figure 8. Difference of horizontal in-situ stress with fluid pressure to that without fluid pressure

The influence of drilling fluid pressure on core discing is more obvious with high in-situ stress. For example, when σ_H reaches 140 MPa, the given σ_L is about 13.2 MPa, but the number of fractures drops to that when σ_H reaches approximately 108 MPa without fluid pressure. Figure 9 compares the result of σ_H reaching 140 MPa and the result of σ_H reaching 108 MPa. Since $N_f^{[1]}$ also reflects the number of complete failures of contact, fractures with 140 MPa is slightly more than that with 108 MPa, but the figure shows that $N_f^{[1]}$ in fig. 9(a) is lower, indicating that fractures of the core with drilling fluid pressure is more dispersed and the extent of stress concentration is lower.

In general, the effect of drilling fluid pressure on core discing does not follow a simple and unidirectional rule. Even when the horizontal in-situ stress is higher than 65 MPa, the given drilling fluid pressure would still produce completely different effects in two in-situ stress sections. However, by further increasing the drilling fluid pressure, core discing would be inhibited eventually. Figure 10 shows the results of the core affected by different fluid pressure in these two sections. It can be seen that the discing phenomenon finally disappears with the increase of fluid pressure.

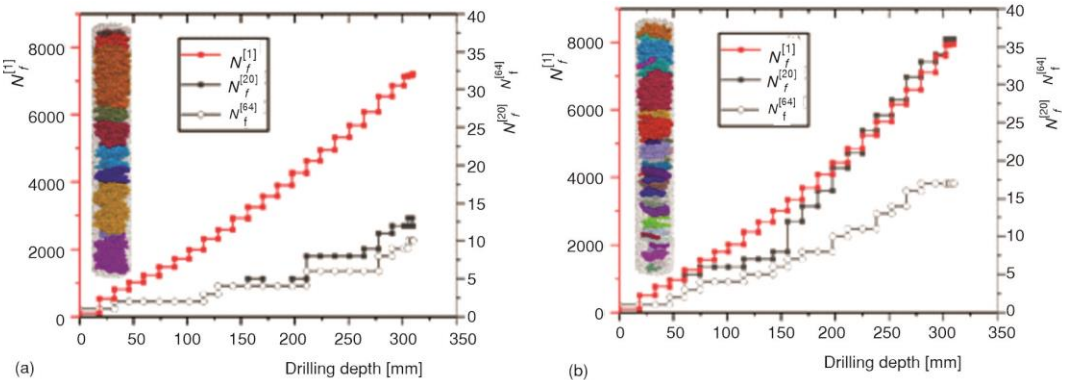

Figure 9. Models and fragment numbers in 140MPa with drilling fluid pressure and 108MPa without drilling fluid pressure; (a) σ_H = 140 MPa, σ_L = 13.2 MPa and (b) σ_H = 108 MPa, σ_L = 0 MPa

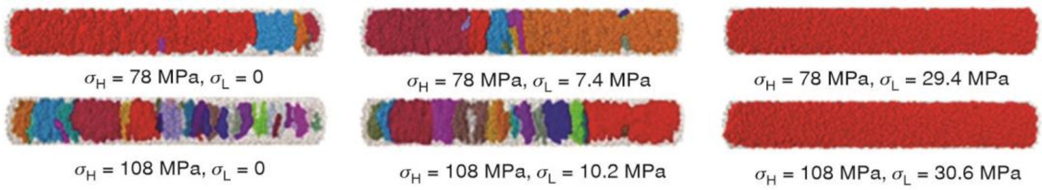

Figure 10. Models with different drilling fluid pressure in conditions of horizontal in-situ stress equal 78 MPa and 108 MPa

Conclusion

Due to the necessary concession of model accuracy in the consideration for computing resources, a finer section of core discs is not shown, and it is not possible to accurately determine whether more saddle surfaces have been generated. The length of discs in a single core is not uniform as in most former simulations but varies with drilling depth. It is impossible to obtain a certain value from the length of core disc to reflect the magnitude of in-situ stress. Even for the most basic conclusion that the higher the stress, the thinner the rock discs [10], different results are obtained in low stress simulation presented in this paper. The comparison of the two values, the drilling depth reflecting the time and the core depth reflecting position, indicates the time when core discing occurs. In almost all the results, the discing occurred when the bit reached its position, indicating that the protection of the core after coring was unable to prevent core discing. The inhibitory effect of drilling fluid pressure on core discing does exist, although the rule is non-linear. If conditions permit, conscious control of drilling fluid pressure can prevent core discing. In the presence of drilling fluid, the core will release the remaining stress during lifting, which can be prevented by adopting pressure-preserved coring. However, it is necessary to verify how core fracture occurs during drilling fluid pressure relief and whether it will lead to further core discing.

Acknowledgment

This work was financially supported by Shenzhen National Science Fund for Distinguished Young Scholars (RCJC20210706091948015) and the National Natural Science Foundation of China (U2013603).

References

[1] Gao, M. Z., *et al.*, Principle and Technology of Coring with In-situ Pressure and Gas Maintaining in Deep Coal Mine (in Chinese), *Journal of China Coal Society*, *46* (2021), 3, pp. 885-897
[2] Gao, M. Z., *et al.*, The Novel Idea and Technical Progress of Lunar In-situ Condition Preserved Coring, *Geomechanics and Geophysics for Geo-Energy and Geo-Resources*, *8* (2022), 2, 20
[3] Lu, Y. Q., *et al.*, The Dynamic Asymmetric Fracture Test and Determination of the Dynamic Fracture Toughness of Large-diameter Cracked Rock Specimens, *Thermal Science*, *23* (2019), Suppl. 3., pp. S897-S905
[4] Gao, M. Z., *et al.*, Calculating Changes in Fractal Dimension of Surface Cracks to Quantify How the Dynamic Loading Rate Affects Rock Failure in Deep Mining, *Journal of Central South University*, *27* (2020), 10, pp. 3013-3024
[5] Gao, M. Z., *et al.*, Mechanical Behavior of Coal under Different Mining Rates: A Case Study from Laboratory Experiments to Field Testing, *Int. J. of Mining Science and Tech.*, *31* (2021), 5, pp. 825-841
[6] Gao, M. Z., *et al.*,The Mechanism of Microwave Rock Breaking and Its Potential Application to Rock-breaking Technology in Drilling, *Petroleum Science*, *19* (2022), 3, pp. 1110-1124
[7] Jaeger, J. C., *et al.*, Pinching-off and Disking of Rocks, *J. of Geophysical Research*, *68* (1963), 6, 1759
[8] Matsuki, K., *et al.*, A Tensile Principal Stress Analysis for Estimating Three-Dimensional In-situ Stresses from Core Disking, *Proceedings*, International Symposium on Rock Stress-RS Kumamoto 97, Kumamoto City Auditorium, Kumamoto, Japan, 1997, pp. 343-348
[9] Dyke, C. G., Core Discing: Its Potential As an Indicator of Principal In Situ Stress Directions, *Proceedings*, ISRM International Symposium, Pau, France, 1989
[10] Obert, L., Stress Conditions under Which Core Discing Occurs, *SME Trans*., *232* (1965), 2, pp. 227-235
[11] Haimson, B. C. Borehole Breakouts and Core Disking as Tools for Estimating in situ Stress in Deep Holes, *Proceedings*, International Symposium on Rock Stress-RS Kumamoto97, Kumamoto City Auditorium, Kumamoto, Japan, 1997, pp. 35-42
[12] Mingzhong, G., *et al.*, Discing Behavior and Mechanism of Cores Extracted from Songke-2 Well at Depths below 4500 m, *Int. Journal of Rock Mechanics and Mining Sciences*, *149* (2022), Jan., 14
[13] Li, Y. Y., *et al.*, Drilling-induced Core Fractures and In situ Stress, *Journal of Geophysical Research-Solid Earth*, *103* (1998), B3, pp. 5225-5239
[14] Hakala, M., Numerical Study of the Core Disk Fracturing and Interpretation of the In situ State of Stress, *Proceedings*, 9th International Congress on Rock Mechanics, Paris, France, 1999, pp. 1149-1153
[15] Yameogo, S. T., *et al.*, Influence of Rock Failure and Damage on In situ Stress Measurements in Brittle Rock, *International Journal of Rock Mechanics and Mining Sciences*, *61* (2013), 2, pp. 118-129
[16] Ma, Z. G., *et al.*, The Mechanism of Fractured Sandstone in Compaction Creep Process, *Thermal Science*, *23* (2019), Suppl. 3., pp. S989-S995
[17] Bahrani, N., *et al.*, Numerical Simulation of Drilling-induced Core Damage and Its Influence on Mechanical Properties of Rocks under Unconfined Condition, *International Journal of Rock Mechanics and Mining Sciences*, *80* (2015), 2, pp. 40-50
[18] Corthesy, R., *et al.*, A Strain-softening Numerical Model of Core Discing and Damage, *International Journal of Rock Mechanics and Mining Sciences*, *45* (2008), 3, pp. 329-350

Paper submitted: August 17, 2022
Paper revised: November 18, 2022
Paper accepted: November 29, 2022